

# Title of the document

TU Delft, Faculty of Applied Sciences,  
BSc program Applied Physics

Delft, April 3rd 2020  
van Loon, Reinaart  
Sangers, Jeroen

## Abstract

The report starts with a Samenvatting (Abstract). The abstract should be self-contained, i.e. a reader should be able to fully understand it without any prior knowledge about the research. Also, in the abstract there should be no references to (figures, tables, formulas etc. in) the remainder of the report, nor to the literature. The abstract tells the reader:

- (1) which research question has been studied,
- (2) what the research method/approach was,
- (3) which results have been obtained, and
- (4) what the main conclusions were.

# Contents

<b>Abstract</b>	i
<b>Table of contents</b>	ii
<b>1 List of symbols</b>	1
<b>2 Introduction</b>	2
<b>3 Theory</b>	3
<b>4 Experimental method</b>	4
4.1 Calibration . . . . .	4
4.2 Microscopic size measurements . . . . .	4
4.3 Birefringence . . . . .	4
<b>5 Results and discussion</b>	6
5.1 Calibration . . . . .	6
5.2 Size measurements . . . . .	6
5.3 Birefringence . . . . .	7
5.4 Resolving power . . . . .	7
<b>6 Conclusions</b>	10
<b>List of references</b>	i
<b>Appendices</b>	i
Appendix A Leica DM EP manual . . . . .	i
Appendix B Calibration . . . . .	iv
Appendix C Size Measurements . . . . .	v

## 1 List of symbols

bla bla bla

bbb

## 2 Introduction

Microscopes are used extensively in natural sciences. They enable us to image small objects and structures which cannot be resolved by the human eye. The use of microscopes, could for example, aid in studies of biological cells, molecular structures or object classification. To correctly conduct such microscopy studies, it is vital to know what the possibilities and limits of the particular microscope are in combination with image improvement techniques.

This experiment will focus on a Leica DM EP polarising microscope in combination with a colour CCD and to what extent this set-up can be used to measure the size of small objects and find the birefringence of an unknown crystal. Furthermore, the possibilities of digital image improvement will be investigated.

After calibrating the pixels and finding the resolving power with the aid of a microscopic ruler and resolution target respectively. Images are made of a human hair, an optical fiber, starch particles, an unknown birefringent crystal and a fungus sample.

To find the size of the human hair, particles and fiber computer techniques will be used. The birefringence of the crystal will be determined by focussing on the differently coloured layers of the crystal, this way we can determine the thickness of each layer and its colour to subsequently calculate the birefringence. Finally some python algorithms are implemented on the image of the fungus to investigate improvements on contrast and colour corrections

In section 2 the theory regarding the experiment will be described, followed by the experimental method in section 3. The results and discussion can be found in section 4. Lastly the conclusions in section 5.

### 3 Theory

A polarizing microscope is used for the experiments in this report. In this section the basic principles of a polarizing microscope and the theory that is used for the experiments are described.

#### 3.0.1 Microscopy

Most modern microscopes are compound microscopes. These type of microscopes can achieve a relatively high angular magnification for nearby objects (Hecht, 2016). For this system, an objective, being the entrance pupil of the system, creates a real inverted, magnified image. The eyepiece creates a virtual images with greater magnification which can be viewed comfortably. The total magnification of the microscope is the product of the individual magnifications of the eyepiece and objective (Hecht, 2016). See figure 1 for a schematic drawing of a basic compound microscope.

#### 3.0.2 CCD recording

In this experiment it was chosen to use a CCD camera to record the imaged from the microscope. To measure distances in a sample it is possible to convert a distance in pixels,  $n_{pixels}$ , to physical unit such as meters. For this, we need a conversion factor that gives the length in meters per pixel,  $l_{pixel}$ . The physical distance,  $d_{physical}$  can easily be calculated using equation 1.

$$d_{physical} = l_{pixel} \cdot n_{pixels} \quad (1)$$

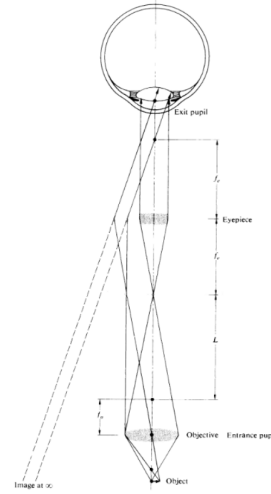


**Figure 1:** Schematic drawing of a compound microscope.  $f_e$  and  $f_o$  correspond to respectively to the focussing distance of the eyepiece and objective. This figure was apdapted from [?].

## 4 Experimental method

This experiment consists of four parts. First the calibration of the microscope. Secondly size measurements on respectively a human hair, an optical glass fibre and starch particles. Thirdly determining the birefringence of an unknown crystal and finally the computerized improvement of an image of a biological fungus sample. The different experimental methods will be treated separately.

The microscope that is used in all experiments is a Leica DM EP microscope. Its manual can be found in appendix 6. This microscope is used in combination with  $4\times$ ,  $10\times$ ,  $40\times$  Hi Plan POL objectives with respectfully a 0.10, 0.22 and 0.65 numerical aperture. A color ccd camera in combination with NI Vision Assistant software is used to acquire digital images.

### 4.1 Calibration

A microscopic ruler is used to measure the length that corresponds to one pixel in an image,  $l_{pixel}$ . This is achieved by focussing on a 1 mm, 100 division ruler and measuring the distance between two focussed, distant division lines and comparing the number of pixels to the physical length. The NI software is used to find the exact location of these two lines and subsequently find the perpendicular projection (see Figure ??). This procedure is repeated for all three objectives. The relative magnification between two objectives,  $M_{A,B}$  can subsequently be found using equation ??.

With the aid of a 1951 USAF resolution target, the resolving power of each objective can be found. First taking a focussed grayscale image on the target and then taking a perpendicular intensity profile for each well defined three-bar structure (see Figure ??). The visibility can subsequently be calculated with equation ?? and the corresponding spatial frequency. This is repeated for all three objectives.

### 4.2 Microscopic size measurements

All microscopic size measurements are made by measuring pixels and comparing this to the corresponding pixel length. This is done for images with the  $40\times$  objective since this gives the smallest error.

#### 4.2.1 Human hair and optical glass fibre

Measuring the thickness of the human hair and optical glass fibre is done with the aid of the NI Vision software. First finding the two straight lines of the outer edges and subsequently measuring the perpendicular distance between the two,  $n_{hair}$  and  $n_{gf}$  in pixels. The actual size,  $l_{hair}$  and  $l_{gf}$ , and error can be calculated using respectfully equation ?? and ??.

#### 4.2.2 Starch particles

In order to measure the size of individual starch particles, a small amount of starch is mixed with oil and images are taken at different locations in the mixture. For ellipse-shaped particles that are focussed in the image, an ellipse can manually be fitted. Using the values for the major and minor axis, respectfully  $a$  and  $b$ , the estimated errors and equations ?? and ??, the area of the ellipse,  $A$ , and corresponding error can be calculated.

For this experiment it was chosen to find the ellipse size for 30 particles.

### 4.3 Birefringence

In order to find the birefringence,  $\Delta n$ , of the unknown crystal, it is placed in the microscope with the polariser crossed with respect to the analyser. The crystal is then turned until bright colours can be seen. Now the difference in path length,  $\Delta l_{path}$ , is measured as a function of the thickness,  $D$ , of the crystal.  $D$  can be found by viewing a border between adjacent colour planes and subsequently

noting the focussing position,  $f$ , of each colour plane. Taking the difference between two values of  $f$  will give the difference in thickness,  $d$ , between two colour planes. The bottom of the sample (black) is also to be taken into account with the same procedure as described above. The birefringence can subsequently be found using orthogonal distance regression with equation ?? and the acquired data.

For this experiment it was chosen to find  $D$  and  $\Delta l_{path}$  for 5 colour planes. The focussing process was repeated 4 to 5 times for every border that was studied.

## 5 Results and discussion

### 5.1 Calibration

The values that have been found for  $l_{real}$ ,  $n$ ,  $l_{pixel}$  and the corresponding error are presented in table 1 for each objective. It was estimated that  $u(n) = 4$ .

The images corresponding to each measurement are presented in figures 8, 9 and 10 in appendix ??.

**Table 1:** Results of measurements of  $n$  for the corresponding value of  $l_{real}$  for each objective. The values for  $l_{pixel}$  and  $u(l_{pixel})$  follow from respectfully equation ?? and ??.

Objective	$l_{real}(m) \cdot 10^{-3}$	$n$	$l_{pixel}$	$u(l_{pixel})$
4×	1	$6.85 \cdot 10^2$	$1.461 \cdot 10^{-6}$	$9 \cdot 10^{-9}$
10×	0.8	$1.247 \cdot 10^3$	$6.42 \cdot 10^{-7}$	$2 \cdot 10^{-9}$
40×	0.2	$1.250 \cdot 10^3$	$1.600 \cdot 10^{-7}$	$5 \cdot 10^{-10}$

The values that have been found for  $M_{A,B}$  for the different objective combinations are presented in table 2.

**Table 2:** Calculated values for  $M_{A,B}$  for the three different objective combinations.

Objective A	Objective B	B/A	$M_{A,B}$	$u(M_{A,B})$
×4	×10	2.5	2.28	$2 \cdot 10^{-2}$
×4	×40	10	9.13	$6 \cdot 10^{-2}$
×10	×40	4	4.01	$2 \cdot 10^{-2}$

As expected, the accuracy for the higher magnification objectives is better. Meaning that images from an objective with a higher magnification, corresponds with a smaller value for  $l_{pixel}$ . However, taking into account the error, not all the values of  $M_{A,B}$  match the theoretical relative magnification of  $\frac{B}{A}$ .

since only the values of  $M_{A,B}$  with  $B = 40$  do not match the theoretical relative magnification, it would suggest that only the ×40 objective is not true to its specifications. More research should be done to prove this.

Apart from the fact that the objectives might not be true to specifications, this does not affect the results of this experiment. It proves, however, the importance of calibrating a microscopy set-up in order to get valid size measurements.

The values that have been found for  $I_{max}$ ,  $I_{min}$ ,  $V_{is}$  and the corresponding errors are presented in table ?? in appendix ???. In figure ??,  $V_{is}$  is plotted as a function of the spatial frequency for each objective. The images corresponding the measurements are presented in appendix ??, ?? and ??.

### 5.2 Size measurements

The values that have been found for  $d_{hair}$  and  $d_{gf}$  are respectively  $d_{hair} = 6.57 \pm 0.08 \cdot 10^{-5} m$  and  $d_{gf} = 1.26 \pm 0.01 \cdot 10^{-4} m$ . The images used for the measurements are presented in appendix Appendix C.

The errors of the values for  $d_{hair}$  and  $d_{gf}$  are in the order of 1 %. Furthermore, the values for  $d_{hair}$  and  $d_{gf}$  are of expected magnitude.

The values for  $a$ ,  $b$ ,  $A$ , the corresponding errors and the corresponding images that have been used can be found in appendix Appendix C. A histogram of the values for  $A$  is presented in figure 2.

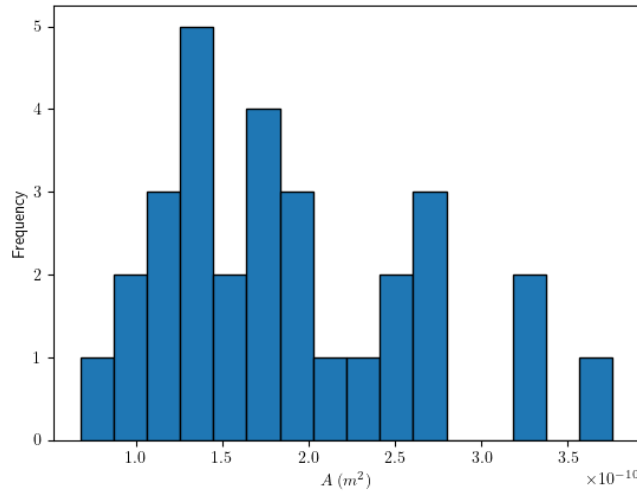


**Figure 2:** Histogram of the values of  $A$  for 30 starch particles.

### 5.3 Birefringence

The colour planes that were taken into account for this experiment can be seen in figure 3 in which each Roman numeral corresponds to a colour plane.

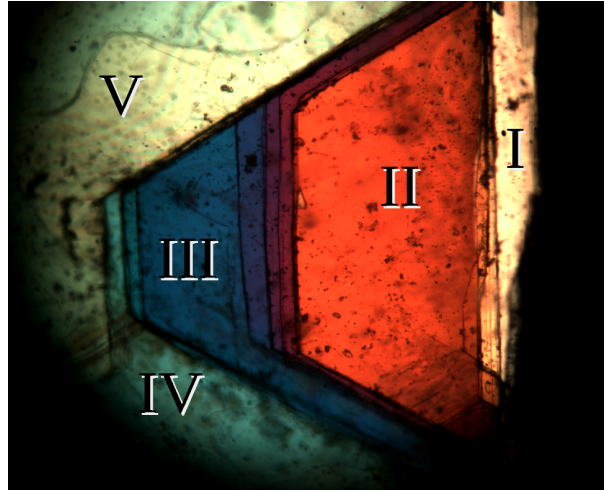


**Figure 3:** Image of a birefringent crystal in a polarizing microscope. The Roman numerals correspond to the different colour planes that were taken into account for this experiment.

The values that have been found for  $f$ ,  $\Delta d$ ,  $D$  and the corresponding errors are presented in appendix ??.

In figure ??,  $\Delta d$  is plotted as a function of  $D$ .

It follows from the orthogonal distance regression that  $\Delta n = 6.6 \pm 0.3 \cdot 10^{-2}$ .

### 5.4 Resolving power

The above photos are the result of the process outlined in the previous section. The high and low values of the line trace were manually read off the photos and entered into a python script capable of calculating the visibility values for each magnification and spatial frequency. The result of which

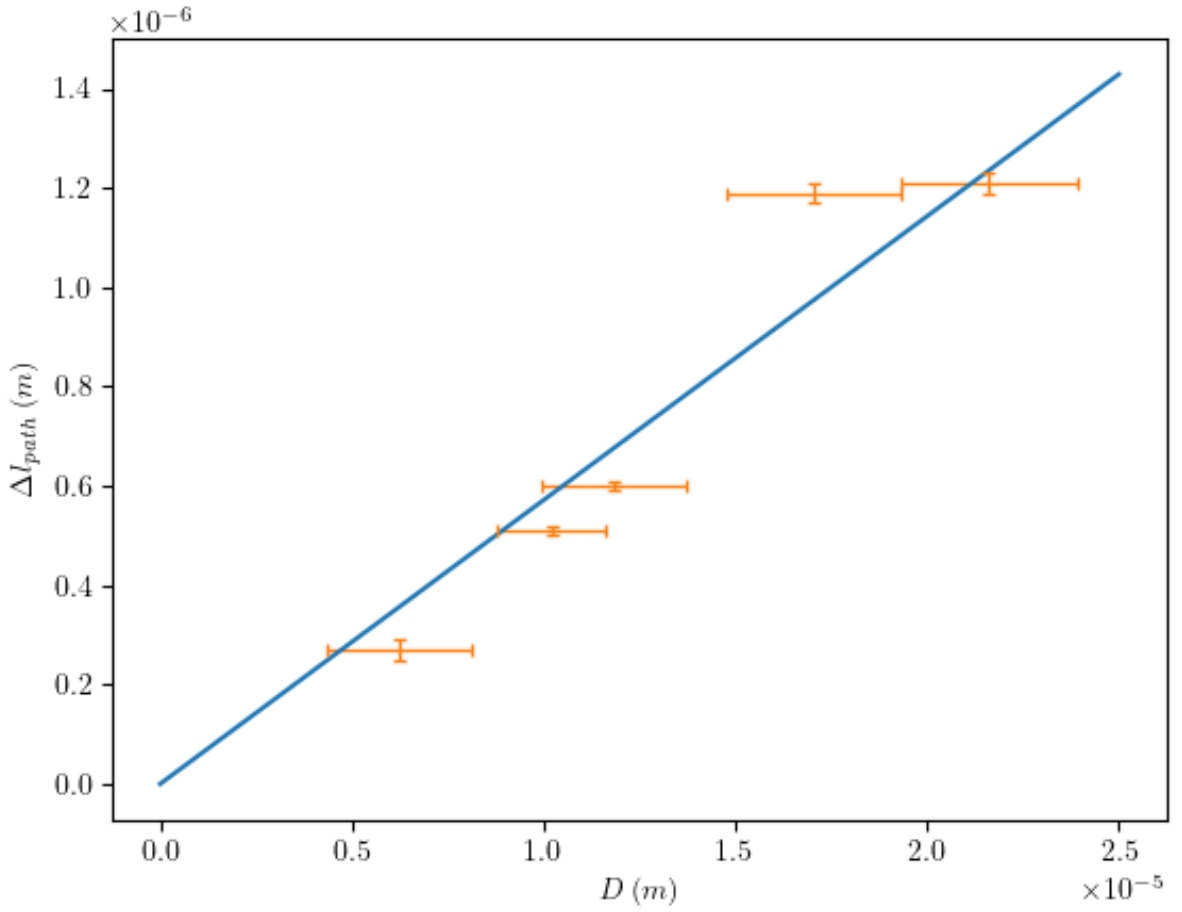


**Figure 4:**  $\Delta l_{path}$  plotted as a function of  $D$ . The data points have errorbars in  $\Delta l_{path}$  and  $D$ . The straight line is a best fit to the data according to an orthogonal distance regression using equation ??.

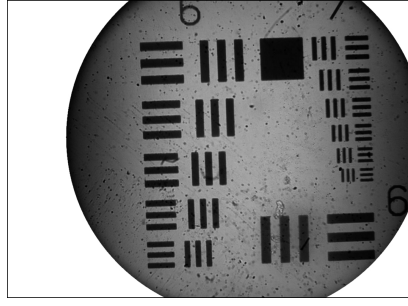


**Figure 5:** Black and white photo.

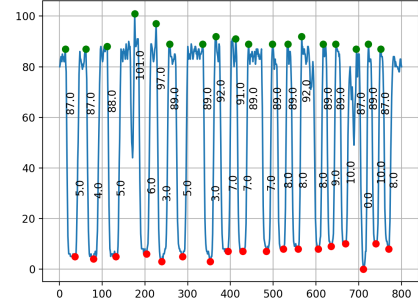
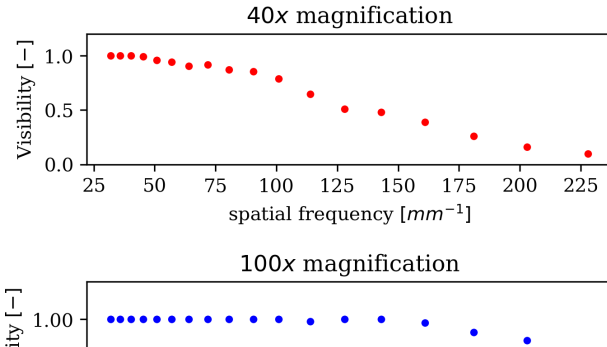


**Figure 6:** Linetrace of seventh group.

can be seen in figure 7.



The data is plotted in such a way that the highest subplot has the lowest magnification and the lowest subplot has the highest magnification. Each subplot has the dimensionless visibility number

plotted on the vertical axis and the spatial frequency plotted on the horizontal axis. We chose this layout since we expect the visibility to decrease when the lines get closer together and the spatial frequency thusly increases. Note that only the verticle visibility axis of the highest subplot starts with a visibility of zero.

What we see is not surprising when we also take into account the photos in the appendix. As can be seen on these photos the highest magnification lense has the smallest numerical aperature, therefore all three traced groups are clearly resolvable. Thus the visibility won't drop as much as the lowest magnification lense when the spatial frequency increases.

Something noticeable however is that the highest magnification plot starts of with the lowest visibility value. This has to do with the fact that this smaller aperature aslo catches less light, the brightest spot in

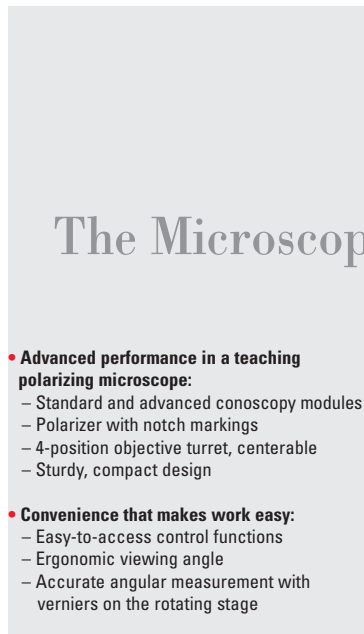
its photo is evidently less bright than that of the other two aperatures. This can be seen when taking a look at either the linetraces or the photos in the appendix.

## 6 Conclusions

In the Conclusions (Conclusions) chapter

- You give a clear and concise answer to the research question that was formulated in the Introduction
- You discuss to what extent, and why, your findings do (not) agree with theory/expectations/earlier work, you discuss more speculative conclusions, and you may do suggestions for further (improved/extended) research. The Conclusions should be self-contained and understandable for readers that have only read the introduction (and have not read the rest of your report, do not know the literature, do not know the experimental setup and have not read the RP manual). In the Conclusions chapter, you may not make references to graphs, tables, equations etc. in the remainder of the report.

## Appendix A Leica DM EP manual



Developed for college teaching and research use:  
the Leica DM EP.

## Leica DM EP

### The Microscope for Teaching and Research

#### Accurate and versatile for teaching

The Leica DM EP is the ideal polarizing microscope for university and other instructional use, offering a standard and an advanced Bertrand lens module for unsurpassed ease of operation. With a wide range of accessories and Leica's renowned optics, the Leica DM EP is exceptional not only for its compact, durable design, but also for its efficiency and ease of operation.

#### Designed for optical brilliance and long life illumination

The standard Köhler field diaphragm and magnetically fixed blue filter provide vivid, pin-sharp images. The 2,000-hour, 35-watt halogen lamp saves hundreds of dollars in replacement bulb cost over the life of the microscope. An illuminated intensity control system reminds the user to switch off the lamp after finishing work to increase the lamp's service life and save energy.



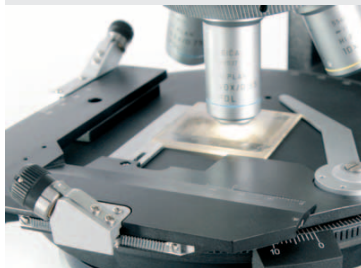
Maximum ease of use and high optical brilliance are  
the outstanding features of the Leica DM EP.

# Modular, Customized Configurations – Microscopes Designed for You

- **Flexibility that gives the freedom you need:**
  - Wide selection of POL objectives
- **Compatibility that knows no bounds:**
  - Fully compatible components across Leica's polarizing microscope product line
  - Wide selection of analyzers, polarizers, and compensators
  - Full wave & quarter wave plates are available
  - Wide selection of POL observation tubes



The result of combining maximum precision and optimum ergonomic design – the 360° analyzer.



Flexibility is key. All of Leica's rotating stage polarizing microscopes feature attachable, interchangeable mechanical stages.

## Flexibility – Designed for you

Flexible to the last detail. All Leica polarizing microscope components can be configured for all microscopes in the polarizing line. For example, you can choose from over twenty POL objectives for the Leica DM4500 P, DM2500 P or DM EP. The optical possibilities are unlimited. You will enjoy the benefits provided by this complete system when using the new 360° analyzer, the 360° polarizer or even with full wave plates. All components can be used for classroom teaching, everyday routine work, and research.

Leica's entire line of DIN standard compensators can be used in all Leica polarizing microscopes, as can the attachable mechanical stage for accurate sample positioning. This always ensures flexible interchange and replacement of parts.

## Technical Data

	Leica DM EP	Leica DM2500 P	Leica DM4500 P
• <b>Objective turret</b>	4x (M25), centerable	5x (M25), centerable	6x (M25), centerable, absolute encoded
• <b>Objectives</b>	HI Plan POL N Plan POL  Immersion objectives	HI Plan POL N Plan POL PL Fluotar POL Immersion objectives	HI Plan POL N Plan POL PL Fluotar POL Immersion objectives
• <b>Usable field of view</b>	20 mm	25 mm	25 mm
• <b>Contrast method</b> Changeover Color reproduction	Manual	Manual	Motorized CCIC: Constant Color Intensity Control
Transmitted light	Polarization contrast Orthoscopy Conoscopy Brightfield Phase contrast	Polarization contrast Orthoscopy Conoscopy Brightfield Phase contrast DIC	Polarization contrast Orthoscopy Conoscopy Brightfield Phase contrast DIC
Incident light	Darkfield Polarization contrast Brightfield	Darkfield Polarization contrast Brightfield Darkfield* DIC Fluorescence	Darkfield Polarization contrast Brightfield Darkfield* DIC Fluorescence
• <b>Conoscopy</b>	Bertrand lens cube in new IL axis Bertrand lens module (AB module) Advanced conoscopy module	Bertrand lens cube	Fully integrated conoscopy beam path User guidance with display feedback
• <b>Transmitted light axis</b> Illumination Operation	12 V 35 W halogen lamp Manual User guidance with CDA	12 V 100 W halogen lamp Manual User guidance with CDA	12 V 100 W halogen lamp Motorized Integrated illumination manager
• <b>Incident light axis</b>	Manual User guidance with CDA	Manual User guidance with CDA	Motorized Integrated illumination manager, round and rectangular field diaphragms for ocular or camera observation
• <b>Condensers</b>	Manual changeover User guidance with CDA	Manual changeover User guidance with CDA	Motorized changeover of condenser head, 7x condenser disc, polarizer
• <b>Focus drive</b>	Manual, 2-gear gearbox	Manual, height-adjustable, Focus stop, 2 or 3-gear gearbox	Manual, 2-gear gearbox

\* on request

## Appendix B Calibration

The three images that are used to find  $l_{pixel}$  for each objective can be found in figure ??, ?? and ??.

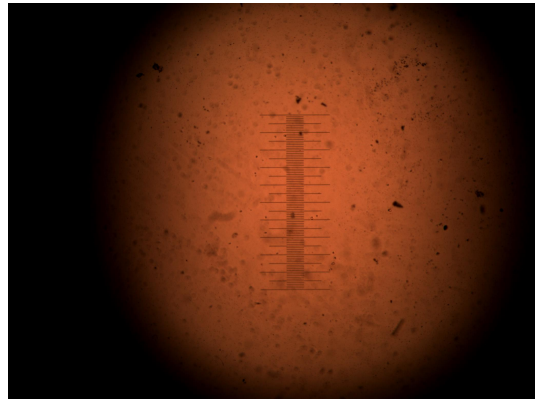


**Figure 8:** Image used to find  $l_{pixel}$  for the  $4\times$  objective.

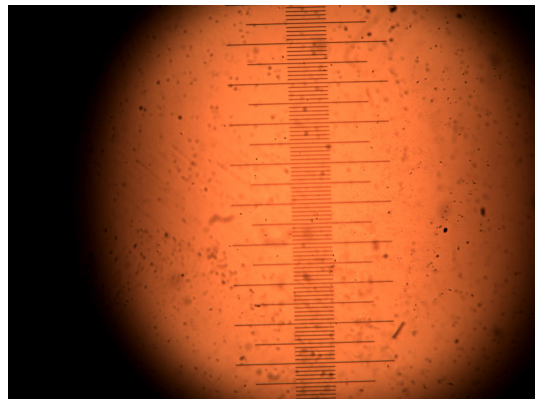


**Figure 9:** Image used to find  $l_{pixel}$  for the  $10\times$  objective.

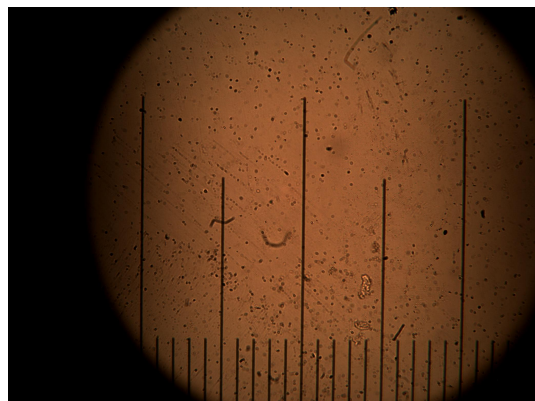


**Figure 10:** Image used to find  $l_{pixel}$  for the  $40\times$  objective.

## Appendix C Size Measurements

The images used to find  $d_{hair}$  and  $d_{gf}$  are presented in respectively figure 11 and 12

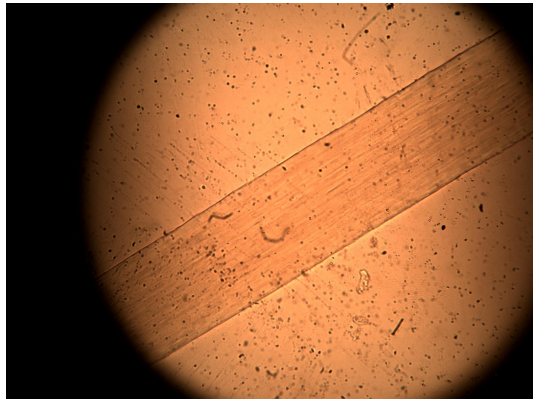


**Figure 11:** Image used to find  $d_{hair}$ .

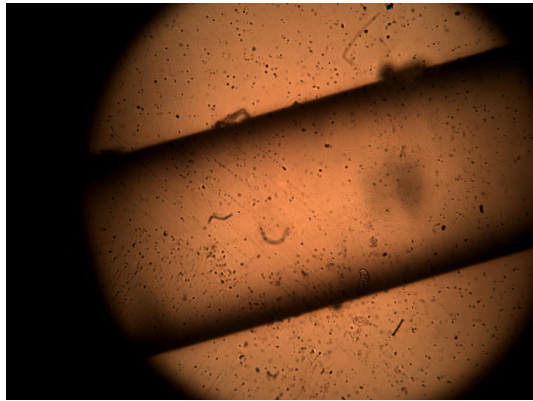


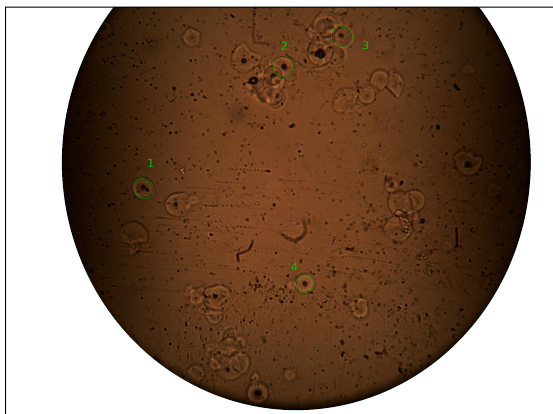
**Figure 12:** Image used to find  $d_{gf}$ .

The values that have been found for  $a$ ,  $b$ ,  $A$  and the corresponding errors are presented in table 3.

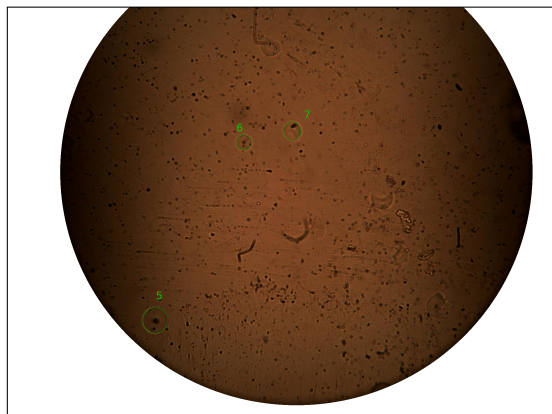
**Table 3:** Results of measurements of  $a$  and  $b$  for 30 starch particles. It was estimated that  $u(a) = u(b) = 2\text{pixels}$ . The values for  $A$  and  $u(A)$  follow from respectfully equation ?? and ???. The particles corresponding to each number can be seen in figures 13a to 13f.

Particle number	$a$ (#pixels)	$b$ (#pixels)	$A \cdot 10^{-10} (\text{m}^2)$	$u(A) \cdot 10^{-12} (\text{m}^2)$
1	84	76	1.28	5
2	83	75	1.25	5
3	85	77	1.32	5
4	72	67	0.97	4
5	97	94	1.83	6
6	58	58	0.68	3
7	70	66	0.93	4
8	105	95	2.01	6
9	92	90	1.67	5
10	84	82	1.39	5
11	115	115	2.66	7
12	146	128	3.76	8
13	119	110	2.63	7
14	76	75	1.15	4
15	112	108	2.43	6
16	127	125	3.19	7
17	99	90	1.79	6
18	84	81	1.37	5
19	135	123	3.34	8
20	80	78	1.26	5
21	86	84	1.45	5
22	112	106	2.39	6
23	105	103	2.18	6
24	74	72	1.07	4
25	117	116	2.73	7
26	90	83	1.50	5
27	100	91	1.83	6
28	117	104	2.45	6
29	100	97	1.95	6
30	99	92	1.83	6

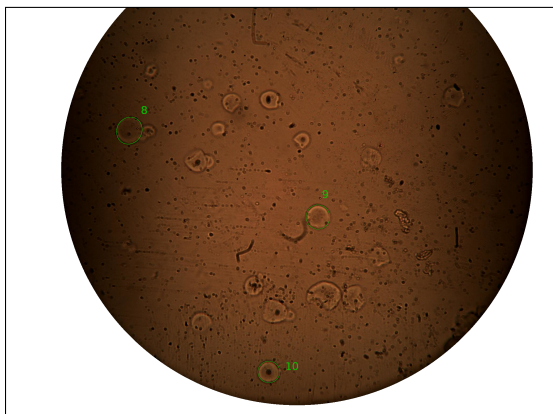
The images that were used to find the data in table 3 can been seen in figure 13



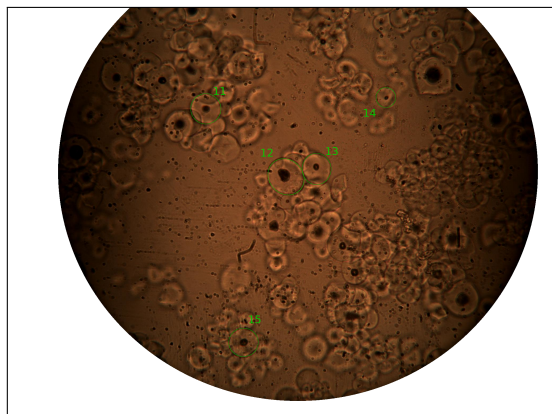
(a) Best ellipse fits for starch particles 1 to 4.



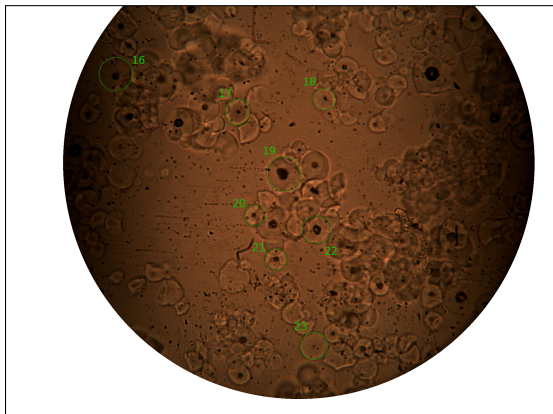
(b) Best ellipse fits for starch particles 5 to 7.



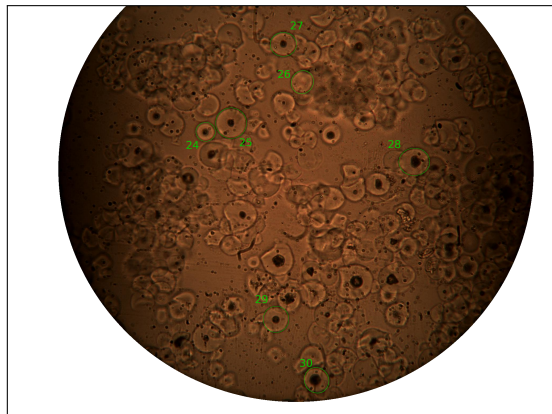
(c) Best ellipse fits for starch particles 8 to 10.



(d) Best ellipse fits for starch particles 11 to 15.



(e) Best ellipse fits for starch particles 16 to 23.



(f) Best ellipse fits for starch particles 24 to 30.

**Figure 13:** Set of images used to find best ellipse fits for 30 starch particles. The green ellipses represent the best fit.